Article

The Effects of Module Temperature on the Energy Yield of Bifacial Photovoltaics: Data and Model

Marco Leonardi [1,2,*], Roberto Corso [1,2], Rachela G. Milazzo [1], Carmelo Connelli [3], Marina Foti [3], Cosimo Gerardi [3], Fabrizio Bizzarri [4], Stefania M. S. Privitera [1] and Salvatore A. Lombardo [1]

1   Institute for Microelectronics and Microsystems (IMM), National Research Council (CNR), Strada VIII, 5, 95121 Catania, Italy; roberto.corso@phd.unict.it (R.C.); gabriella.milazzo@imm.cnr.it (R.G.M.); Stefania.Privitera@imm.cnr.it (S.M.S.P.); salvatore.lombardo@imm.cnr.it (S.A.L.)
2   Department of Physics and Astronomy, University of Catania, Via S. Sofia, 64, 95123 Catania, Italy
3   Enel Green Power, Contrada Blocco Torrazze, Zona Industriale, 95121 Catania, Italy; carmelo.connelli@enel.com (C.C.); marina.foti@enel.com (M.F.); cosimo.gerardi@enel.com (C.G.)
4   Enel Green Power, Viale Regina Margherita 125, 00198 Rome, Italy; fabrizio.bizzarri@enel.com
*   Correspondence: marco.leonardi@phd.unict.it

Abstract: Bifacial photovoltaics (BPVs) are emerging with large momentum as promising solutions to improve energy yield and cost of PV systems. To reach its full potential, an accurate understanding of the physical characteristics of BPV technology is required. For this reason, we collected experimental data to refine a physical model of BPV. In particular, we simultaneously measured the module temperature, short circuit current (I_{sc}), open-circuit voltage (V_{oc}), power at the maximum power point (P_{mpp}), and the energy yield of a bifacial and a monofacial minimodule. Such minimodules, realised with the same geometry, cell technology, and module lamination, were tested under the same clear sky outdoor conditions, from morning to afternoon, for three days. The bifacial system experimentally shows higher module temperatures under operation, about 10 °C on a daily average of about 40 °C. Nevertheless, its energy yield is about 15% larger than the monofacial one. We propose a physical quantitative model that fits the experimental data of module temperature, I_{sc}, V_{oc}, P_{mpp}, and energy yield. The model was then applied to predict the annual energy yield of PV module strings. The effect of different PV module temperature coefficients on the energy yield is also discussed.

Keywords: bifacial PV modelling; temperature effect; NOCT model

1. Introduction

The bifacial photovoltaic (BPV) system represents a promising technology for the future development of photovoltaics (PVs). Bifacial solar cells simultaneously collect incident solar radiation from the sun on the front side, such as conventional monofacial PV (MPV), and the albedo radiation from the ground on the back, plus some additional diffused light. Therefore, compared with MPV, under suitable conditions, BPV can effectively increase the energy yield of PV modules and strings at reduced costs. Since BPV presents the possibility to reduce the levelised cost of energy (LCOE), the International Technology Roadmap for Photovoltaics has predicted for the bifacial technology an increase in the worldwide market share from 30% in 2020 to about 80% by 2031 [1].

Several BPV technologies are available on the market. These include the passivated emitter rear contact (PERC) cells, the passivated emitter rear totally diffused (PERT) cells, and the silicon heterojunction technology (HJT) cells. Differences in cell structure result in different values of the bifaciality factor (BF), defined as the ratio of the power at the maximum power point (MPP) measured on the back divided to the front-side power at MPP under standard test conditions (STC). Generally, the BF ranges between 70% and 100% depending on the technology (PERC, PERT, HJT, etc., see [2,3]). Among the HJT cells,

the n-type ones are the most promising for BPV, due to their high short-circuit current (I_{sc}), open-circuit voltage (V_{oc}), and BF, and for their low temperature coefficient [4] compared with the most common p-type cells [5].

In parallel to experimental studies, relevant efforts have been dedicated to the modelling of bifacial devices. Yusufoglu et al. [6] proposed a model to predict the annual energy yield based on the calculation of the ground-reflected radiation reaching the rear side of the PV module. A further refinement of the model has been developed to take into account the uneven radiation distribution on the back surface of the PV module [7]. A method to evaluate the bifacial gain (BG) for different installations was proposed by Shoukry et al. [8]. Sun et al. [9] studied the optimisation of a stand-alone bifacial module for various geographic locations. In our previous works [10,11], we have proposed an analytical model which considers the spectral content of the solar radiation incident on the front and back surfaces of PV modules. This model has been validated on experimental data and applied to evaluate inhomogeneous illumination on large PV strings and energy yield of BPV systems, either with fixed-tilt installation or uniaxial trackers. In particular, we found that, provided that the strings have sufficiently large open perimeters, the fixed installations produce a similar energy yield, compared with the same strings installed with uniaxial solar trackers.

When modelling BPV systems, module temperature is a key aspect to consider since, in most PV technologies, a high temperature negatively affects the energy yield. Hence, a reliable prediction of the BPV energy yield has to correctly evaluate the total impinging solar radiation as well as the module temperature. On the one hand, the BPV module temperature is expected to be higher since the PV module collects the solar radiation both from the front side and from the back, and since most of this power is transformed into a heat flux, a higher module temperature is foreseen. On the other hand, an opposite argument concerns the absorption of the impinging IR portion of the spectrum. Since the bifacial cells, contrarily to the Al back surface field (Al-BSF) monofacial cells, are more transparent in the IR, less solar radiation energy is effectively collected by the bifacial cell, resulting in a lower cell temperature. Lamers et al. [12] analysed the impact of IR radiation on Al-BSF MPV modules. In this case, at low albedo, the MPV module temperature is estimated to be higher, compared with the BPV system. Only at high rear side irradiances did the authors estimate that the BPV system becomes hotter than the monofacial one. Similar results were also reported by Zhang et al. [13], who refined the previous studies by considering also the case of different ground albedos. Patel et al. [4] underlined the role of the IR sub-bandgap absorption, which increases the PV module temperature under bifacial operation. These works show the importance of using technologies with power temperature coefficients low in absolute value, such as in the case of Si HJT.

Previous works [12–14] have studied a direct comparison of performance and module temperature in bifacial and monofacial modes. In these studies, the differences in module temperature are due to the differences in the solar irradiation in MPV and BPV, but they are also heavily influenced by the different technologies used to realise the modules. A comparison in which only the operation mode (bifacial or monofacial) is varied but the Si PV technology is maintained the same is needed, to isolate the role played by the type of irradiation (front and back vs. only front).

In summary, the problem of predicting the PV module temperature in BPV is a crucial aspect which needs further analysis. In this paper, we report an experimental study focused on this problem, and on the basis of the experimental results, we refine the physical model that we have previously proposed [10,11] which calculates the BG in three-dimensional system geometry.

The experiments were performed in clear-sky outdoor conditions and focused on a direct comparison of two minimodules of three cells realised by the same bifacial HJT technology, one of them operating in bifacial mode and the other one operating simultaneously in monofacial mode. The physical quantities of interest include minimodule temperature, I_{sc}, V_{oc}, power at the maximum power point (P_{mpp}), and energy yield. By comparing

minimodules realised by the same PV technology, the differences in module temperature can only be ascribed to the differences in the mode in which the solar radiation impinges on the modules.

The proposed refinement to the model is an equation to estimate the BPV module temperature that takes into account the additional light collected by the module back. We validate the updated model by using the experimental data of the minimodules reported below. In the final part of the paper, we use the model to predict the yearly energy yield and the effect of varying the power temperature coefficient.

2. Experimental

Two identical minimodules of 3 bifacial n-type Si HJT cells were prepared. The HJT cell, characterised by a hydrogenated amorphous Si/crystalline Si heterojunction, is based on a technology developed by Enel Green Power at its 3SUN facility. Under STC, these cells show a V_{oc} of 730 mV, an I_{sc} of 9.3 A, a BF of 90%, and a power conversion cell efficiency (PCCE) of 22.7%. We realised our minimodules by connecting 3 cells in series with copper strips and laminating them in a double transparent polyethylene substrate with EVA backing. One of the modules was covered with white cardboard on the back to completely prevent the albedo light collection. In this way, the module operated similarly to a monofacial module with a white back sheet. In fact, the white cardboard here used has a low transmittance in the infrared range while, in some cases, the infrared white back sheets transmittance can be quite large [15], which would likely imply a better thermal behaviour of the module.

The minimodules were tested in outdoor conditions in Catania, Italy (37°26′ N, 15°4′ E). The data were collected from about 9 a.m. to 4 p.m. for 3 days in the period from 17 to 19 February 2021, on sunny days with no clouds.

An image of the minimodules during the experiments is shown in Figure 1. The module height (55 cm) and orientation (35° inclination from ground, modules facing south) were chosen to optimise front- and back-side solar radiation and ground albedo collection, according to our previously developed model [10]. The chosen height did not correspond to the maximum PV energy yield but rather to the point where the further height increase produced only a marginal improvement of energy yield [16].
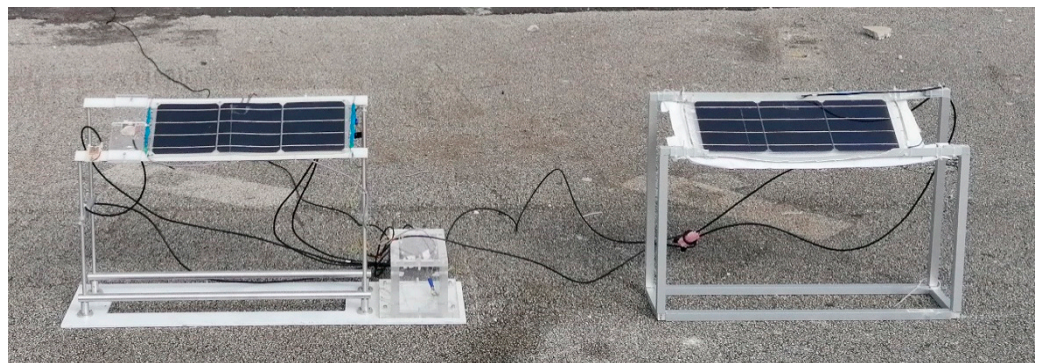

Figure 1. Image of the experimental setup: front view of the two minimodules, with the bifacial on the left and the monofacial on the right.

The minimodules were placed on a piece of asphalt which shows an average normal incidence reflectivity of 30% over the 300–1100 nm range, as reported in Privitera et al. [16].

The solar irradiation intensity impinging on the PV minimodules (Efront) was measured by using an MS-40 EKO pyranometer. The pyranometer was tilted at 35° similar to the minimodules. In addition, the minimodule temperatures were measured by using two very small thermo-resistances directly placed in close thermal contact to the front and back of each minimodule. These probes were covered with white cardboard to shield the solar radiation. Overall, each thermo-resistance had a size of 4 mm2, and it was placed above the PV cell bus bars, thus producing negligible PV cell shadowing.

Figure 2 shows an example of the temperatures measured on the front (T_{front}) and back (T_{back}) surfaces of the module over time during one day of measurements, on both bifacial and monofacial minimodule.
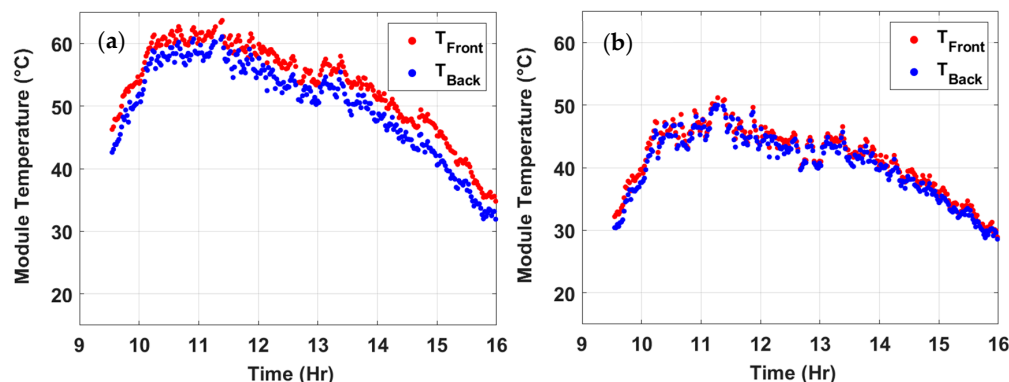

Figure 2. Example of measured temperatures of the minimodule on the front and back surfaces as a function of time for bifacial (**a**) and monofacial (**b**) minimodule measured in one of the days of measurement.

In all cases, T_{Front} is larger than T_{Back}. This is most likely mainly due to the different amounts of solar radiation impinging on the front and back surfaces of the PV minimodules, evidenced by the very different short circuit current levels measured in bifacial and monofacial systems at all times, as shown in the next section.

Given that the minimodule structure is symmetric, with both sides laminated with the same process, we assumed that the module temperature (T_{module}) is the average of the temperatures measured on the front and on the back, that is,

$$T_{module} = \frac{T_{front} + T_{back}}{2} \tag{1}$$

More complex models of module temperature have been formulated which implement heat transmission throughout the module [17]; however, glass–glass commercial modules usually have thicknesses starting from 4 mm, while our minimodule is only 1 mm thick and is encapsulated in a polyethylene substrate, as stated above. For these reasons, we assumed the simpler approach of Equation (1).

From Figure 2, it is clear that the bifacial module temperature is higher than that of the monofacial module. This was systematically observed in all cases, and it will be discussed in detail in the following parts of the paper.

The current–voltage (I–V) characteristic of each PV minimodule was measured by a Kelvin configuration. For each minimodule, the current was evaluated by the voltage drop across a 20 mΩ resistor connected in series. The voltage across the module was swept by a variable load, obtained by an STP60NF06 power MOS repeatedly driven from OFF to ON condition by a linear staircase signal at 0.2 Hz applied to the transistor gate. Data were continuously acquired through a USB-6343 National Instrument data logger.

In the module bias region between ≈1.8 V and ≈2 V, the I–V data were affected by noise due to the acquisition system, and these data points were eliminated and excluded from further data analysis. Nevertheless, it has to be noted that such data filtering did not have any impact on the measurement of I_{sc}, V_{oc}, and P_{mpp}. All these parameters were reliably measured from the experimental I–V curves such as those of Figure 3. Each I–V trace was repeatedly taken on each 90 s, obtaining 250 data sets on average during each day. With this setup, we could follow the daily evolution of the PV system characteristics with high time resolution and an accuracy in the measurements of current and voltage of about 0.5% and 0.1%, respectively. Finally, the ambient temperature data were collected from an in situ weather station.
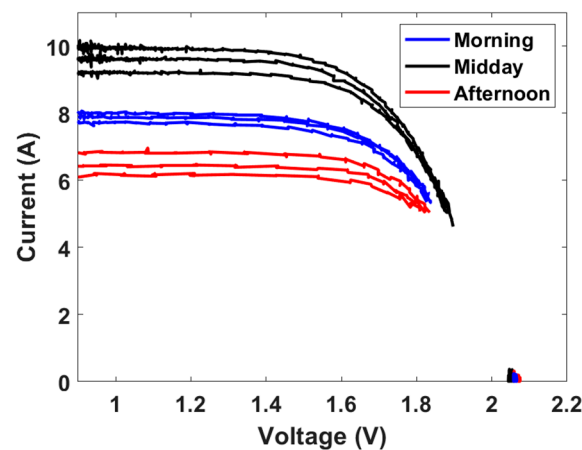
Figure 3. Experimental I–V curves collected from the bifacial minimodule in one of the days of measurements.

3. Results and Discussion

3.1. Module Temperature

Figure 4b reports the experimental data of the PV minimodule temperature of both modules and of the ambient temperature (T_{amb}), averaged over the three days of measurements. As expected, temperatures are lower in the morning, reach their maximum at midday, and decrease in the afternoon. Module temperatures are much higher than the ambient temperature since solar irradiation warms up the modules. In particular, it is evident that the bifacial module is up to about 12 °C warmer than the monofacial module. This behaviour, systematically observed and quite remarkable, was quantitatively modelled, as discussed in Section 3.3 of this paper, by using Equations (2) and (3). In fact, Figure 4 also shows the module temperature profiles, calculated according to the proposed model, which reproduces quite well the experimental trends: this is true for the average values as well as for the temperatures measured on a single specific day (17 February 2021) with an RMSE of 7.3% of experimental values for the bifacial minimodule and 11.7% for the monofacial minimodule.
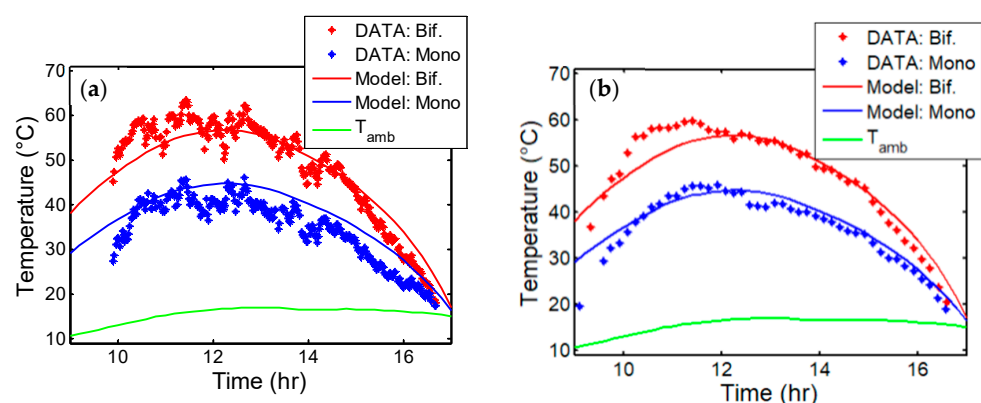

Figure 4. Data of a single day of module temperature compared with the values predicted by the model (**a**) and average values compared with the model (**b**). Ambient temperature is also reported as reference.

3.2. Module Electrical Parameters

Figures 5b, 6b and 7b report, respectively, the experimental data of I_{sc}, V_{oc}, and electrical energy yield at the maximum power point as a function of time averaged in the 3 days of measurements. For this experiment, we define the energy yield as the cumulative energy produced by the minimodule at its maximum power point since the start of the

measuring period (about 9 a.m.). The figures also report the calculated curves of the best fit of the model to the experimental data. In particular, Figure 5 also reports the calculated contribution to the bifacial PV module I_{sc} due to the albedo light collection by the back of the PV cell (green continuous line). The I_{sc} difference in bifacial and monofacial modules is due to the contribution of the current collected by the back of the PV module. The latter, compared with the monofacial module I_{sc} corrected by the PV cell BF, provides an estimate of the ratio of the solar radiation flux collected by the back surface (A_{bot}) with respect to the one collected by the front A_{top}. A_{bot}/A_{top} was measured by using two photodetectors oriented similarly to the PV minimodules, but one facing up and the other facing down towards the ground (data not shown), which results in the order of 17–20%; that is, the radiation impinging on the back is about 17–20% of the radiation incident on the front. The proposed model captures this feature quite well since, from Figure 5, it is evident that the model and data are in good agreement. The model fits both the average and the chosen day data, with an RMSE of 4.7% and 1.5% for bifacial and monofacial minimodules, respectively.
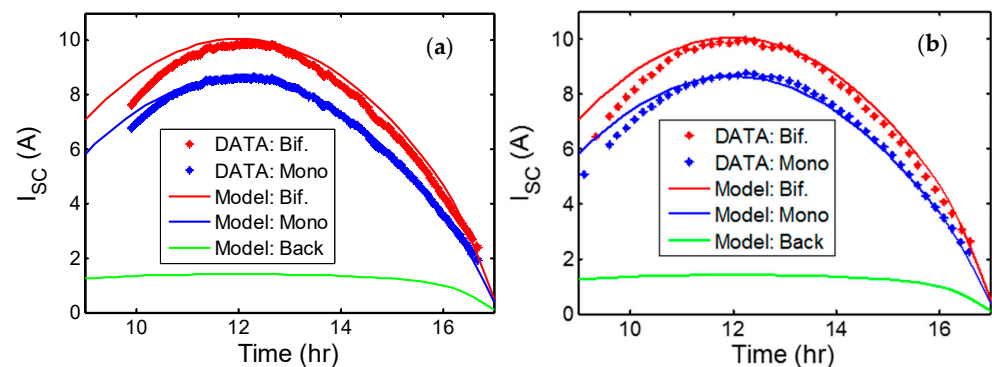

Figure 5. Data of a single day of module I_{SC} compared with the values predicted by the model (**a**) and average values compared with the model (**b**). The model allows also to separately calculate the current generated by the back surface of the module.

Figure 6. Data of a single day of module V_{OC} compared with the values predicted by the model (**a**) and average values compared with the model (**b**).

The results show clearly that the bifacial PV minimodule, compared with the monofacial one, even if it exhibits a larger temperature, has a much larger short circuit current, owing to the albedo light collection by the PV cell's back side, a moderately lower V_{oc}, attributed to the larger module temperature, and a remarkably larger energy yield at the maximum power point.
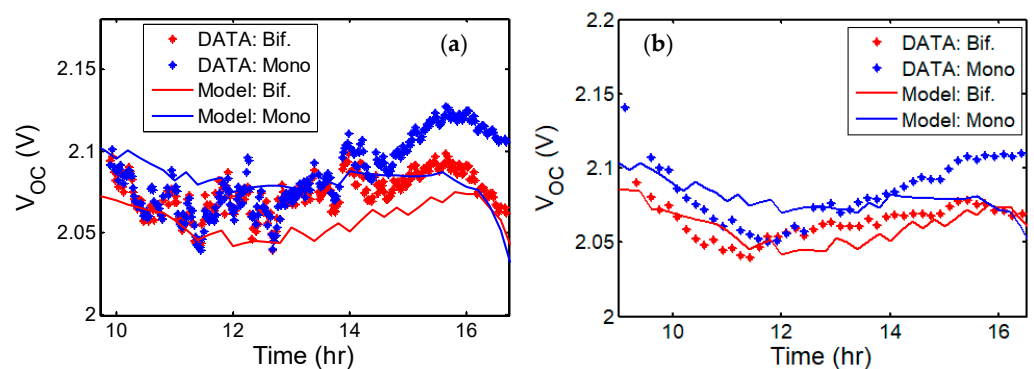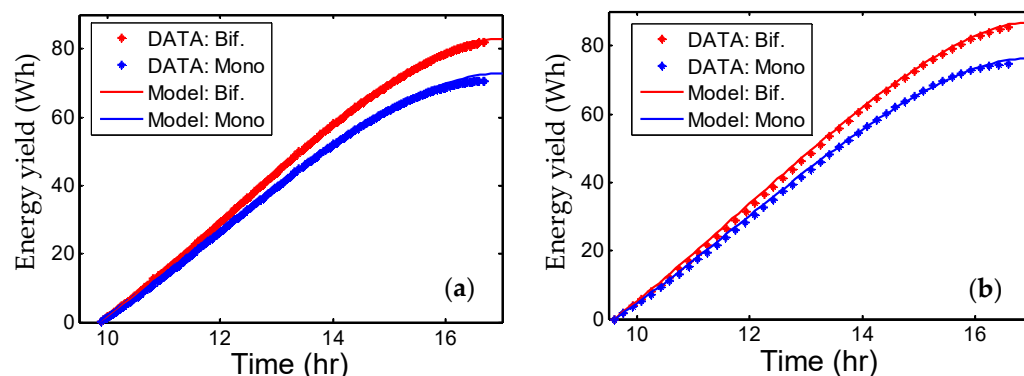
Figure 7. Data of a single day of module energy yield compared with the values predicted by the model (**a**) and average values compared with the model (**b**).

Figures 5–7 also report the calculated best-fit curves of the quantitative model described below, which allows performing quantitative evaluations of the energy yield of bifacial PV systems. A good match of the experimental data to the model curves is evident. Similar to procedures for the other quantities, the model was tested against the average data and data of the chosen day: for the V_{oc} value, we obtained an RMSE of 0.8% for the bifacial minimodule and 0.9% for the monofacial minimodule, while for the energy yield, we obtained an RMSE of 2.4% and 2.1% for bifacial and monofacial minimodules, respectively. In the next section, we describe the proposed model and report its evaluations of bifacial PV annual energy yields as a function of the PV module's temperature coefficients.

3.3. Model of Bifacial PV and Data Fitting

In refs. [10,11], we have proposed a model to evaluate the I–V characteristics and energy yield of PV bifacial modules and strings. The model assumes a complete three-dimensional (3D) geometry, that is, no simplification to a bidimensional (2D) approximation is carried out. While differences in back-side irradiance, due to the position of the modules in the string, can be neglected for longer strings, this is not the case for shorter strings [18]. It takes into account the impinging solar radiation divided into the direct, diffuse, and reflected components, modelled by using the ASHRAE model [19], the Global Solar Atlas database [20], Liu and Jordan's isotropic model of diffused light [21], and the nominal operating cell temperature (NOCT) model [22]. The solar radiation impinging on the bifacial PV device was separated into two parts, that is, the I_{sc} component due to the solar radiation impinging on the front $I_{sc,front}$, and the I_{sc} component due to the albedo radiation diffused by the ground, $I_{sc,back}$. $I_{sc,front}$ was calculated by considering only the direct and the diffused radiation incident on the front, exactly in the same way as in the case of the monofacial solar cells. Vice versa, $I_{sc,back}$ was calculated only in the case of bifacial modules, and it was obtained by integrating over all the elements of the ground on which the PV system was installed, which all act as isotropic light sources diffusing light proportionally to the global horizontal radiation and to the ground albedo. More specifically, $I_{sc,front}$ was calculated as the convolution of the front side external quantum efficiency (EQE) with the spectrum of the solar radiation incident to the front, while $I_{sc,back}$ was calculated as the integral over all the underlying ground elements of the radiation diffused by each element, proportional to the solid angle under which it sees the solar cell back. Further details of the model are reported in [11]. In the calculation, we took into account the wavelength dependence of ground albedo, back-side EQE, and the spectrum of the horizontal component of the solar spectrum. A larger ground area was considered to correctly evaluate the back-side irradiance of outermost modules. The model also took into account when the incident radiation has a large incidence angle on the receiving PV surface element, to correct for the increasing reflectivity which reduces the actually collected radiation.

Once for each cell the overall I_{sc} was calculated as the sum of $I_{sc,front}$ and $I_{sc,back}$, as reported in more detail in [10], the cell current–voltage (I–V) characteristics were calculated according to the well-known current source/single-diode lumped element circuit model of the PV cell [23]. The I–V curve of the PV module or of the PV string was then numerically calculated by considering the series of all the PV cells. In the present case, this corresponded to numerically calculating the series of 3 cells in the case of the minimodule and of 432 cells in the case of the string of 6 PV modules; then, the V_{oc} was obtained as the PV system voltage corresponding to a current equal to 0 A, while the P_{mpp} was evaluated as the maximum of the power produced by the system.

The PV cell lumped element model requires the cell temperature which, therefore, needs to be correctly modelled. Several temperature models have been defined over the years, both for commercial modules and single cells [24]. One of the main factors that differentiate these models is whether they take into account the effect of wind or not. As our outdoor measurements were performed under light breeze conditions [25], quite close to those used to measure the NOCT, we chose to start from the NOCT model and adapt it to describe our experiment. Although a comprehensive analysis of the diverse temperature models is beyond the scope of this work, it has to be noted that models that include wind may be even less accurate than those that do not consider this factor, especially in non-windy locations [26]. Moreover, the NOCT parameter is usually used for commercial and industrial purposes, and for this reason, a correction that extended the model to BPV would be desirable. In the experiments here reported, we experimentally measured the PV module temperatures both in bifacial and monofacial cases, and we observed noticeable differences, as shown in Figures 2 and 4. Therefore, to take into consideration the large observed temperature difference, we refined the model of refs. [10,11] as follows: in a conventional monofacial PV module the temperature is evaluated as

$$T_{mono} = T_{amb} + E_{front} \cdot (NOCT_{mono} - 20)/800, \qquad (2)$$

where E_{front} is the intensity of the solar radiation impinging on the PV cell front, to be expressed in W/m^2, while $NOCT_{mono}$ is the nominal operating condition temperature to be expressed in °C.

We assumed that Equation (2) is only valid for monofacial PV modules, while for the case of bifacial modules, we also had to consider the radiation impinging on the back. In fact, in monofacial modules, the radiation impinging on the module's back surface is mostly reflected away by the white back sheet and therefore it does not contribute to the module temperature. We believe that this is the reason for the large differences observed experimentally between monofacial and bifacial modules (Figures 2 and 4). Based on such premises, we introduced an equation similar to Equation (2) as follows:

$$T_{bm} = T_{amb} + (E_{front} + E_{back}) \cdot (NOCT_{bif} - 20)/800 \qquad (3)$$

where T_{bm} is the temperature of the bifacial PV module, and $NOCT_{bif}$ is the NOCT of the bifacial PV module. As far as the radiation impinging on the back surface is concerned, rather than simply adding such radiation to E_{front}, we believed that it is more accurate to account for this additional term by calculating the ratio between $I_{sc,back}$ and $I_{sc,front}$, as each factor already considers the radiation that is actually absorbed by the respective side of the cell. In fact, as stated above, one of the factors in the calculation of I_{sc} is the EQE, which is different for each side and excludes from the calculation the fraction of irradiance that is reflected or transmitted which does not contribute to cell heating.

Therefore, by assuming the model above described refined with Equations (2) and (3), we calculated the best-fit curves of the model to the data of Figures 4–7.

The fit parameters are the $NOCT_{bif}$, $NOCT_{mono}$, the power temperature coefficient α_T, the STC PV cell I_{sc}, V_{oc}, and the series resistance R_s. All best-fit values are very close to the average values measured for unencapsulated cells in STC [27]. Slight changes of the order of 10% around the STC values were allowed for V_{oc} and I_{sc}. On the contrary, for the R_s

parameter, an increase up to a factor 3 of the STC value was allowed. The R_s best-fit value ($2\times$ the STC value) found is likely due to the bus bar and lamination processes which can produce some worsening of the series resistance. The best-fit values used for the curves calculated in Figures 4–7 are reported in Table 1.

Table 1. Best-fit values of the proposed model compared with the STC cell values.

Parameter	Best-Fit Value	Measured STC Value
PV cell I_{sc}	9.15 A	9.30 A
PV cell V_{oc}	720 mV	730 mV
PV cell R_s	6 mΩ	3 mΩ
PCCE at maximum power point	21.1%	22.7%
α_T	$-0.26\%/^\circ$C	$-0.26\%/^\circ$C
Mini-module NOCT$_{mono}$	42 $^\circ$C	-
Mini-module NOCT$_{bif}$	47 $^\circ$C	-

As evident from Table 1, it is found that the cell best-fit values correspond to lower performances compared with the cell parameters measured in STC. This is likely due to the non-standard minimodule fabrication and lamination process which produce some worsening compared with unencapsulated cell parameters [28].

Nevertheless, the best-fit values are quite close to the initial STC cell parameters, and the resulting curves calculated by the proposed model reproduce the experimental data well, in terms of PV system energy yield as well as by closely following the data of the other fundamental physical parameters (module temperature, V_{oc}, I_{sc}).

It has to be noted that the best-fit value of NOCT$_{bif}$ is larger than that of NOCT$_{mono}$. This result can be explained by considering the definition of NOCT, which is the operating condition temperature of the module when irradiated at 800 W/m^2, at 45° inclination, at an ambient temperature of 20 $^\circ$C, and with a wind flowing at 1 m/s. Given the definition, it appears realistic that NOCT$_{bif}$ would be larger than NOCT$_{mono}$ since, under solar irradiation, the bifacial module collects the albedo light from the ground. This is, on the contrary, mostly reflected away by the monofacial module which has a white back sheet. Therefore, more solar power is collected by the bifacial module, producing a larger temperature.

3.4. Model Extrapolations to Annual PV Energy Yield and Effect of α_T

By using the proposed model, the results of the present experiments can be extrapolated to realistic conditions, considering PV module strings of many modules rather than minimodules of a few cells and yearly energy yields rather than daily yields. For this purpose, we chose a realistic PV system configuration also in terms of the size of the ground directly illuminated by the sun contributing to the albedo collected by the bifacial system. In a previous paper [10], we have evaluated the effect of such perimeter size, and in the present evaluation, we chose a perimeter size large enough to reach the maximum possible gain of the BPV energy yield, compared with the monofacial PV.

We evaluated the annual energy yield of the bifacial system, compared with the monofacial one. We chose the latitude of Catania (37°26' N, 15°4' E) and the temperature profile in Catania in the year 2017, as reported in [25]. In all cases, the systems were assumed to be oriented towards the south and with a 35° inclination, similar to the experiments, and because this is the tilt angle to achieve the maximum annual energy yield. Figure 8 reports the relative bifacial gain, defined as

$$\text{BG} = 100 \cdot \frac{\text{EY}_{bif} - \text{EY}_{mono}}{\text{EY}_{mono}} \tag{4}$$

where EY stands for energy yield, according to the temperature profile of Catania in 2017. Two cases were considered: the case of the three-cell minimodule installed at an average height of 55 cm, as in Figure 1 and for the experiments here reported (blue curve), and the case of a string of 6 modules of 72 cells (6 cells high and 12 cells wide) of 1 m × 2 m arranged in a 2 × 3 configuration (2 modules high and 3 modules wide), installed at an average height of 2 m (red curve). Both cases were in a landscape-type installation, i.e., with the PV system long side along the east–west direction.
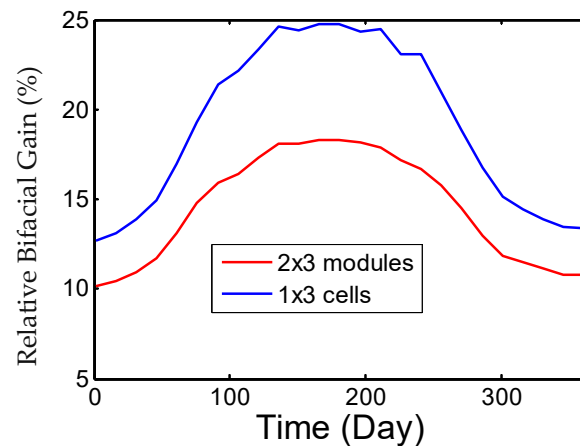

Figure 8. Modelled relative bifacial gain over the course of the year for a minimodule (blue) and a string of six modules (red).

The figure shows clearly that the system with the largest energy yield is the smallest one, i.e., the three-cell minimodule. This was expected since as the size of the PV system size increases, the differences of illumination of the back surfaces of the PV cell become worse, that is, larger. Since all cells are in series, the PV cell with the worst back-side illumination, i.e., the one with the lowest I_{sc} will dominate the energy yield. This effect becomes much stronger for a large string of 6 modules with 432 cells; therefore, the PV relative bifacial gain is clearly lower. Nevertheless, the relative bifacial gain is still quite remarkable, calculated to be always above 10%, with a clear and remarkable advantage of energy yield. Such results are in good agreement with the experimental data reported in refs. [29–31] and with the calculated values reported in refs. [32,33]. We also note that, according to our model, the maximum difference in temperature between bifacial and monofacial modules is between 9 °C and 12 °C at the latitude of Catania throughout the year.

The other aspect that we investigated is the weight of the α_T parameter of the solar cells for the application in the bifacial mode. In general, it is well known that PV technologies with low α_T in absolute value or even positive temperature coefficients are preferable for application in warm climates. This feature is also very useful in the case of bifacial systems. In fact, as we showed here, the temperature of a bifacial module tends to be higher, compared with that of the same module used in monofacial mode with a white surface on the back. Hence, one expects that the relative bifacial gain will be better in technologies with low α_T in absolute value. To quantify the advantage, we performed calculations using the model here proposed.

Figure 9 reports the relative bifacial gain as a function of time calculated for the temperature profile of Catania in 2017 and for the case of one string of 6 modules in 2 × 3 landscape configuration, as previously described. All cases were calculated by assuming the same values of the parameters, as reported in Table 1, except for α_T, which is varied from −0.26%/°C to −0.45%/°C, that is, in the range of the most important silicon PV technologies currently available. As expected, as α_T increases in absolute value the relative bifacial gain decreases. From the best to the worst case, the change is noticeable, of about

−20%. In all cases, however, the bifacial systems show a strong advantage in terms of energy yield.
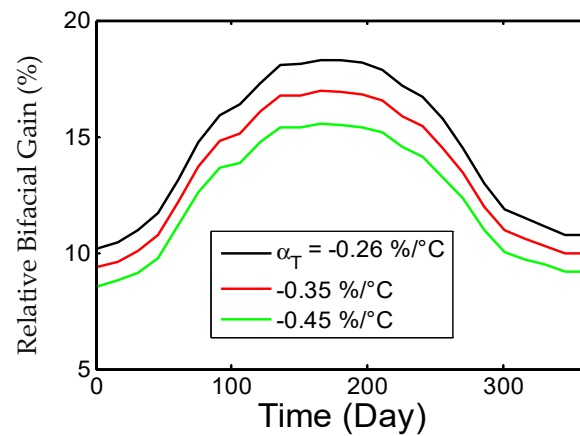

Figure 9. Modelled percent increase in relative bifacial gain over the course of the year of a six-module string for different values of the power temperature coefficient.

In summary, in this work, we experimentally studied and modelled the module temperature for the same bifacial technology used in a bifacial mode or, on the contrary, in a monofacial mode, by covering the module's back surface with a white sheet. We found that the PV module when operated as bifacial exhibits larger temperatures, estimated to be between 9 °C and 12 °C, depending on the season, at midday throughout the year for the latitude of Catania. Nevertheless, the bifaciality provides a noticeable advantage in terms of system energy yield. The PV technologies with low α_T in absolute value provide more advantage when used in bifacial mode. This is, for example, the case of the HJT technology used in the experiments here reported, with an α_T of −0.26%/°C.

4. Conclusions

In this work, we showed, discussed, and quantitatively modelled the results of outdoor tests performed for 3 days in clear sky conditions on two PV minimodules based on Si HJT technology. Rather than monitoring the behaviour of the modules at their maximum power point, we continuously swept the load on the modules from the open- to the short-circuit condition with a 90 s period. This allowed us to monitor V_{oc}, maximum power point, I_{sc}, and module temperature. Using this approach, we directly compared monofacial and bifacial operations within the same Si PV technology, evaluating the quantitative correlation between PV electrical performance, solar irradiance on the PV module front and back, and the module temperature.

The results reveal that the observed increase in power output and consequent better energy yield in the case of bifacial operation is mainly due to the higher short-circuit current. The increase in current is high enough to completely overcome the effect of the higher module temperature and the consequent lower open-circuit voltage observed in bifacial operation.

Owing to the experimental data on PV module temperature, we refined our 3D model to evaluate the PV system's bifacial gain. The model well reproduces the experimental results of module temperature, V_{oc}, I_{sc}, maximum power point, and energy yield, both in monofacial and in bifacial operations. Hence, we used the model to evaluate the annual energy yields and the effect of varying the power temperature coefficient. From such analysis, the n-type HJT technology appears to be particularly suitable for bifacial photovoltaics given its very low temperature coefficient.

References

1. International Technology Roadmap for Photovoltaics, 12th ed. 2021. Available online: https://itrpv.vdma.org/en/ (accessed on 20 February 2021).
2. Liang, T.S.; Pravettoni, M.; Deline, C.; Stein, J.S.; Kopecek, R.; Singh, J.P.; Luo, W.; Wang, Y.; Aberle, A.G.; Khoo, Y.S. A review of crystalline silicon bifacial photovoltaic performance characterisation and simulation. *Energy Environ. Sci.* **2019**, *12*, 116–148. [CrossRef]
3. Gu, W.; Ma, T.; Ahmed, S.; Zhang, Y.; Peng, J. A comprehensive review and outlook of bifacial photovoltaic (bPV) technology. *Energy Convers. Manag.* **2020**, *223*, 113283. [CrossRef]
4. Patel, M.T.; Vijayan, R.A.; Asadpour, R.; Varadharajaperumal, M.; Khan, M.R.; Alam, M.A. Temperature-dependent energy gain of bifacial PV farms: A global perspective. *Appl. Energy* **2020**, *276*, 115405. [CrossRef]
5. Yu, B.; Song, D.; Sun, Z.; Liu, K.; Zhang, Y.; Rong, D.; Liu, L. A study on electrical performance of N-type bifacial PV modules. *Sol. Energy* **2016**, *137*, 129–133. [CrossRef]
6. Yusufoglu, U.A.; Lee, T.H.; Pletzer, T.M.; Halm, A.; Koduvelikulathu, L.J.; Comparotto, C.; Kopecek, R.; Kurz, H. Simulation of Energy Production by Bifacial Modules with Revision of Ground Reflection. *Energy Procedia* **2014**, *55*, 389–395. [CrossRef]
7. Yusufoglu, U.A.; Pletzer, T.M.; Koduvelikulathu, L.J.; Comparotto, C.; Kopecek, R.; Kurz, H. Analysis of the Annual Performance of Bifacial Modules and Optimization Methods. *IEEE J. Photovolt.* **2015**, *5*, 320–328. [CrossRef]
8. Shoukry, I.; Libal, J.; Kopecek, R.; Wefringhaus, E.; Werner, J. Modelling of Bifacial Gain for Stand-alone and in-field Installed Bifacial PV Modules. *Energy Procedia* **2016**, *92*, 600–608. [CrossRef]
9. Sun, X.; Khan, M.R.; Deline, C.; Alam, M.A. Optimization and performance of bifacial solar modules: A global perspective. *Appl. Energy* **2018**, *212*, 1601–1610. [CrossRef]
10. Galluzzo, F.R.; Canino, A.; Gerardi, C.; Lombardo, S.A. A new model for predicting bifacial PV modules performance: First validation results. In Proceedings of the 2019 IEEE 46th Photovoltaic Specialists Conference (PVSC), Chicago, IL, USA, 16–21 June 2019; pp. 1293–1297. [CrossRef]
11. Galluzzo, F.R.; Zani, P.E.; Foti, M.; Canino, A.; Gerardi, C.; Lombardo, S. Numerical Modeling of Bifacial PV String Performance: Perimeter Effect and Influence of Uniaxial Solar Trackers. *Energies* **2020**, *13*, 869. [CrossRef]
12. Lamers, M.W.P.E.; Özkalay, E.; Gali, R.S.R.; Janssen, G.J.M.; Weeber, A.W.; Romijn, I.G.; Van Aken, B.B. Temperature effects of bifacial modules: Hotter or cooler? *Sol. Energy Mater. Sol. Cells* **2018**, *185*, 192–197. [CrossRef]
13. Zhang, Z.; Wu, M.; Lu, Y.; Xu, C.; Wang, L.; Hu, Y.; Zhang, F. The mathematical and experimental analysis on the steady-state operating temperature of bifacial photovoltaic modules. *Renew. Energy* **2020**, *155*, 658–668. [CrossRef]
14. Rodríguez-Gallegos, C.D.; Bieri, M.; Gandhi, O.; Singh, J.P.; Reindl, T.; Panda, S.K. Monofacial vs. bifacial Si-based PV modules: Which one is more cost-effective? *Sol. Energy* **2018**, *176*, 412–438. [CrossRef]
15. McIntosh, K.R.; Jung, J.; Abbott, M.D.; Sudbury, B.A. Determination and evaluation of a backsheet's intrinsic reflectance. *AIP Conf. Proc.* **2018**, *1999*, 020018. [CrossRef]
16. Privitera, S.; Muller, M.; Zwaygardt, W.; Carmo, M.; Milazzo, R.; Zani, P.; Leonardi, M.; Maita, F.; Canino, A.; Foti, M.; et al. Highly efficient solar hydrogen production through the use of bifacial photovoltaics and membrane electrolysis. *J. Power Sources* **2020**, *473*, 228619. [CrossRef]
17. Notton, G.; Cristofari, C.; Mattei, M.; Poggi, P. Modelling of a double-glass photovoltaic module using finite differences. *Appl. Therm. Eng.* **2005**, *25*, 2854–2877. [CrossRef]
18. Marion, B.; MacAlpine, S.; Deline, C.; Asgharzadeh, A.; Toor, F.; Riley, D.; Stein, J.; Hansen, C. A Practical Irradiance Model for Bifacial PV Modules. In Proceedings of the 2017 IEEE 44th Photovoltaic Specialist Conference (PVSC), Washington, DC, USA, 25–30 June 2017; pp. 1537–1542. [CrossRef]

19. American Society of Heating, Refrigerating and Air-Conditioning Engineers. *ASHRAE Handbook, 1985 Fundamentals: An Instrument of Service Prepared for the Profession Containing Technical Information*; The Society: Atlanta, GA, USA, 1985.

20. Global Solar Atlas. Available online: https://globalsolaratlas.info/ (accessed on 20 February 2021).

21. Liu, B.; Jordan, R. Daily insolation on surfaces tilted towards equator. *ASHRAE J.* **1961**, *10*, 53–59.

22. Ross, R.G., Jr. Interface design considerations for terrestrial solar cell modules. In Proceedings of the 12th Photovoltaic Specialists Conference, Baton Rouge, LA, USA, 15–18 November 1976; pp. 801–806.

23. Xiao, W.; Dunford, W.G.; Capel, A. A novel modeling method for photovoltaic cells. In Proceedings of the 2004 IEEE 35th Annual Power Electronics Specialists Conference (IEEE Cat. No.04CH37551), Aachen, Germany, 20–25 June 2004; pp. 1950–1956.

24. Santiago, I.; Trillo-Montero, D.; Moreno-Garcia, I.; Pallarés-López, V.; Luna-Rodríguez, J. Modeling of photovoltaic cell temperature losses: A review and a practice case in South Spain. *Renew. Sustain. Energy Rev.* **2018**, *90*, 70–89. [CrossRef]

25. Weather Underground. 2020. Available online: https://www.wunderground.com/ (accessed on 20 February 2021).

26. Zouine, M.; Akhsassi, M.; Erraissi, N.; Aarich, N.; Bennouna, A.; Raoufi, M.; Outzourhit, A. Mathematical Models Calculating PV Module Temperature Using Weather Data: Experimental Study BT. In Proceedings of the 1st International Conference on Electronic Engineering and Renewable Energy, Saidia, Morocco, 15–17 April 2018; pp. 630–639.

27. Foti, M.; Galiazzo, M.; Cerasti, L.; Sovernigo, E.; Gerardi, C.; Guglielmino, A.; Litrico, G.; Sciuto, M.; Spampinato, A.; Ragonesi, A.; et al. Silicon Heterojunction Solar Module using Shingle interconnection. In Proceedings of the 2021 IEEE 48th Photovoltaic Specialists Conference (PVSC), Fort Lauderdale, FL, USA, 20–25 June 2021; pp. 1092–1095. [CrossRef]

28. Green, M.A.; Dunlop, E.D.; Hohl-Ebinger, J.; Yoshita, M.; Kopidakis, N.; Hao, X. Solar cell efficiency tables (Version 58). *Prog. Photovolt. Res. Appl.* **2021**, *29*, 657–667. [CrossRef]

29. Park, H.; Chang, S.; Park, S.; Kim, W.K. Outdoor Performance Test of Bifacial n-Type Silicon Photovoltaic Modules. *Sustainability* **2019**, *11*, 6234. [CrossRef]

30. Molin, E.; Stridh, B.; Molin, A.; Wackelgard, E. Experimental Yield Study of Bifacial PV Modules in Nordic Conditions. *IEEE J. Photovolt.* **2018**, *8*, 1457–1463. [CrossRef]

31. Jang, J.; Lee, K. Practical Performance Analysis of a Bifacial PV Module and System. *Energies* **2020**, *13*, 4389. [CrossRef]

32. Gu, W.; Li, S.; Liu, X.; Chen, Z.; Zhang, X.; Ma, T. Experimental investigation of the bifacial photovoltaic module under real conditions. *Renew. Energy* **2020**, *173*, 1111–1122. [CrossRef]

33. Abotaleb, A.; Abdallah, A. Performance of bifacial-silicon heterojunction modules under desert environment. *Renew. Energy* **2018**, *127*, 94–101. [CrossRef]